Scattering of 14.1 MeV neutrons by 10B

Autor(en): **Vaucher, B. / Alder, J.C. / Joseph, C.**

Objekttyp: **Article**

Zeitschrift: **Helvetica Physica Acta**

Band (Jahr): **43 (1970)**

Heft 3

PDF erstellt am: **09.08.2024**

Persistenter Link: https://doi.org/10.5169/seals-114167

Nutzungsbedingungen

Die ETH-Bibliothek ist Anbieterin der digitalisierten Zeitschriften. Sie besitzt keine Urheberrechte an den Inhalten der Zeitschriften. Die Rechte liegen in der Regel bei den Herausgebern.
Die auf der Plattform e-periodica veröffentlichten Dokumente stehen für nicht-kommerzielle Zwecke in Lehre und Forschung sowie für die private Nutzung frei zur Verfügung. Einzelne Dateien oder Ausdrucke aus diesem Angebot können zusammen mit diesen Nutzungsbedingungen und den korrekten Herkunftsbezeichnungen weitergegeben werden.
Das Veröffentlichen von Bildern in Print- und Online-Publikationen ist nur mit vorheriger Genehmigung der Rechteinhaber erlaubt. Die systematische Speicherung von Teilen des elektronischen Angebots auf anderen Servern bedarf ebenfalls des schriftlichen Einverständnisses der Rechteinhaber.

Haftungsausschluss

Alle Angaben erfolgen ohne Gewähr für Vollständigkeit oder Richtigkeit. Es wird keine Haftung übernommen für Schäden durch die Verwendung von Informationen aus diesem Online-Angebot oder durch das Fehlen von Informationen. Dies gilt auch für Inhalte Dritter, die über dieses Angebot zugänglich sind.

Ein Dienst der *ETH-Bibliothek*
ETH Zürich, Rämistrasse 101, 8092 Zürich, Schweiz, www.library.ethz.ch

http://www.e-periodica.ch

Scattering of 14.1 MeV Neutrons by ^{10}B

by **B. Vaucher, J. C. Alder** and **C. Joseph**
Institut de physique nucléaire, Université de Lausanne, Suisse

(10. XII. 69)

Abstract. The angular distributions of the differential cross-sections for scattering of 14.1 MeV neutrons to the $Q = 0, -1.74, -2.15, -3.58, -4.77, -(5.11+5.16+5.18), -(5.92+6.04+6.13), -6.56$ and $-(6.88+7.0)$ MeV levels of ^{10}B have been measured for $11° \leqslant \theta_{CM} \leqslant 164°$. They were deduced from the time-of-flight spectra of neutrons scattered by two targets of different ^{10}B and ^{11}B isotopic concentrations, with the help of a Monte-Carlo program which reproduced the measured spectra. Owing to the small values of the measured cross-sections, a precise determination of parasitic events was necessary.

The elastic scattering has been analysed by the optical model. A coherent description of the inelastic scattering to the 2.15, 3.58, 5.16 and 6.56 MeV levels has been achieved with the collective DWBA model. The not yet well-defined parity of the $Q = -6.56$ MeV level appears to be negative.

Introduction

Only few measurements of neutron scattering by ^{10}B and ^{11}B have been made. Elastic scattering has been measured twice at 14 MeV for natural boron [1, 2]. Inelastic scattering on ^{11}B has been measured, also at 14 MeV, with a natural boron target and without isolating the contribution from each level [1]. Inelastic scattering on ^{10}B has been measured in the vicinity of 7 MeV for some levels or groups of levels [3]. An improvement of this situation had been hoped for [4, 5].

As it was not possible to obtain sufficient quantities of isotopically pure ^{10}B and ^{11}B, our measurements were carried out using two targets having different concentrations of ^{10}B and ^{11}B. The time-of-flight method was used. The ^{10}B and ^{11}B levels being very close to each other (Fig. 1), it was difficult to separate in the measured spectra, first, the contribution of each isotope, and second, the contribution of each level of one isotope. Moreover, because of the low values of the cross-sections, a precise determination of parasitic events was necessary.

In this paper, we shall describe the experimental technique and give the results obtained with ^{10}B. The results for ^{11}B will be published elsewhere [6]. A more detailed treatment can be found in references [7, 8].

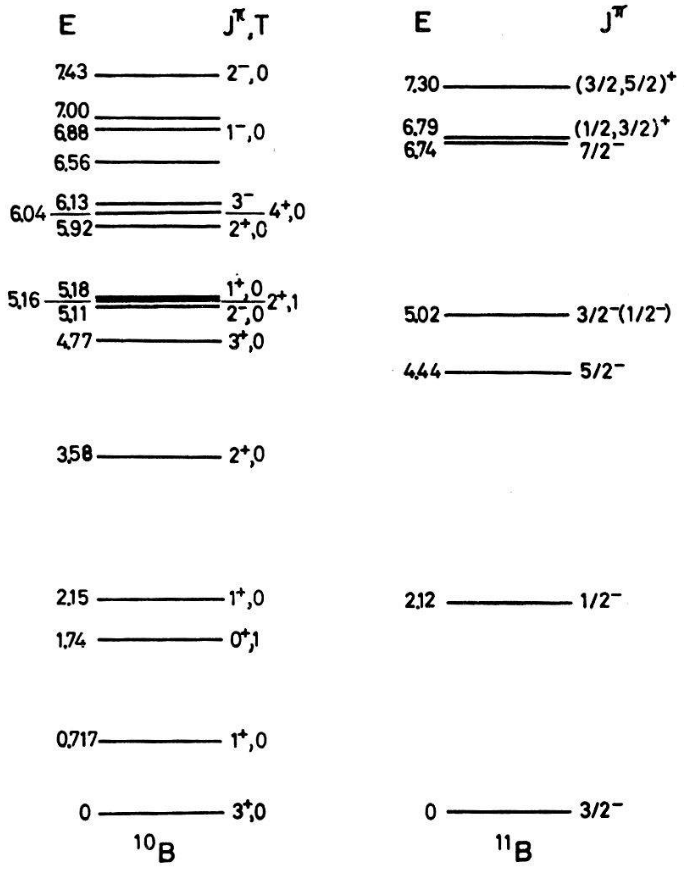

Figure 1
Energy levels of ^{10}B and ^{11}B.

1. Experimental Set-up

The incident neutrons, of 14.15 ± 0.10 MeV, were produced in the reaction ^{3}H$(d, n)^4$He induced by a beam of 145 keV deuterons (diameter of beam: 1.5 mm) striking a thin titanium tritiated target. The α-particles emitted in a solid angle defined by a rectangular aperture 30 mm high and 11.4 mm wide, located 71 mm from the target, were detected, thus defining a neutron beam. The mean angle between the trajectories of the α-particles and the deuteron beam was 92.4°. Two different scatterers, each measuring 7.2 cm high, 1.8 cm wide and 5 cm thick, were used alternately, the center of the scatterer being placed along the neutron beam axis, 18 cm from the source. The first scatterer consisted of natural boron (81.17% ^{11}B; 18.83% ^{10}B), the second was enriched in ^{10}B (91.35% ^{10}B; 8.65% ^{11}B). The interaction rate was the same for both scatterers: of the 70.4 ± 0.8% of the beam neutrons reaching the scatterer, 37% gave rise to an interaction. Because of the closeness of the ^{10}B and ^{11}B levels, a flight path of 4 to 5 m, depending upon the mean scattering angle ϕ_0, was necessary. The neutron detector consisted of an NE 213 liquid scintillator, enclosed in an aluminium cell of rectangular section (19.6 × 20.05 cm), 3.6 cm thick. Its threshold was fixed to detect recoil protons of energy $\geqslant 3$ MeV. A pulse-shape discrimination circuit [9] eliminated most of the events due to γ-rays.

The measurements were carried out for 14 scattering angles in an open geometry. Only a pyramidal iron shadow bar, 25 cm long and with a minimal cross-section, was placed between the source and the neutron detector, as close to the former as possible. The electronic circuitry was of the classical fast-slow type. The time-to-pulse-height converter used has already been described [10].

The time resolution, measured in direct flight, was 1.9 ns at half-maximum and 4.4 ns at 10%. The overall angular resolution was ± 6.5° for forward and back-scattering angles, and ± 5° for medium angles. The half-maximum width of the distribution of effective scattering angles does not vary with ϕ_0 and has a value of ± 4.5°.

2. Parasitic Phenomena

In addition to the neutrons simply and multiply scattered by the boron, the time-of-flight spectra measured with both scatterers contain the following parasitic events:

1. Accidental coincidences: these are uniformly distributed in the measured spectra. Their number was calculated from the individual counting rates. Auxiliary measurements with additional delays to eliminate any time correlation in the analysed region, have confirmed the validity of this evaluation. The resulting uncertainty in the determination of the cross-sections is smaller than 0.1 mb/sr.

2. Scattering by the 50 μm-thick copper enclosure containing the boron powders and by the impurities in the ^{10}B-enriched scatterer (1.9% C; 1.2% O). The time-of-flight spectra of these events have been calculated from known cross-sections. The effect of impurities in the natural boron scatterer (0.3%) was negligible.

3. Contribution from the environment. We group under this heading the following two processes: a) neutrons from the incident beam scattered by the air and b) events resulting from two successive interactions, the first one in the scatterer, the second one in any material inside the experimental hall (air, walls, etc.). These two processes have been measured together, by using an iron shield, 50 cm long, to stop almost all the neutrons between the scatterer and the detector (transmission $< 1^0/_{00}$). After subtraction of the accidental coincidences, the residual spectrum is equivalent to the contribution from the environment to the total spectrum of the scatterer. Process b) is the more important one, and essentially consists of two successive elastic scattering events. Nonetheless, a non-negligible contribution results from the detection of γ's emitted in reactions induced in the experimental hall matter by neutrons elastically scattered inside the scatterer (the pulse shape discrimination system not being perfect).

Thus, the contribution from the environment depends essentially upon the probability for elastic scattering in the scatterer. Since the total macroscopic cross-sections and the angular distributions of the elastic differential scattering cross-sections are quite similar for both scatterers, the contribution from the environment hardly depends upon the scatterer, as we have verified experimentally. It is therefore sufficient to measure it for one scatterer only.

3. Measurement

For each of the 14 scattering angles ϕ_0 chosen, three spectra have been measured, namely the total spectrum from each scatterer and the spectrum of the contribution from the environment. The length of each measurement varied from 48 hours for the forward angles to 96 hours for the backward angles. The α-particle detection rate was 10^4 s^{-1}, corresponding to a total source intensity of 1.85×10^6 neutrons per second over 4π sr.

In Figure 2, we have plotted the three spectra measured for $\phi_0 = 40°$, as well as the calculated spectrum of the scattering by the impurities and the enclosure for the ^{10}B-enriched scatterer. From this set of spectra, we deduced by subtraction the two spectra from which the cross-sections were calculated, namely the spectra containing only simple and multiple scattering from the two boron isotopes in each scatterer.

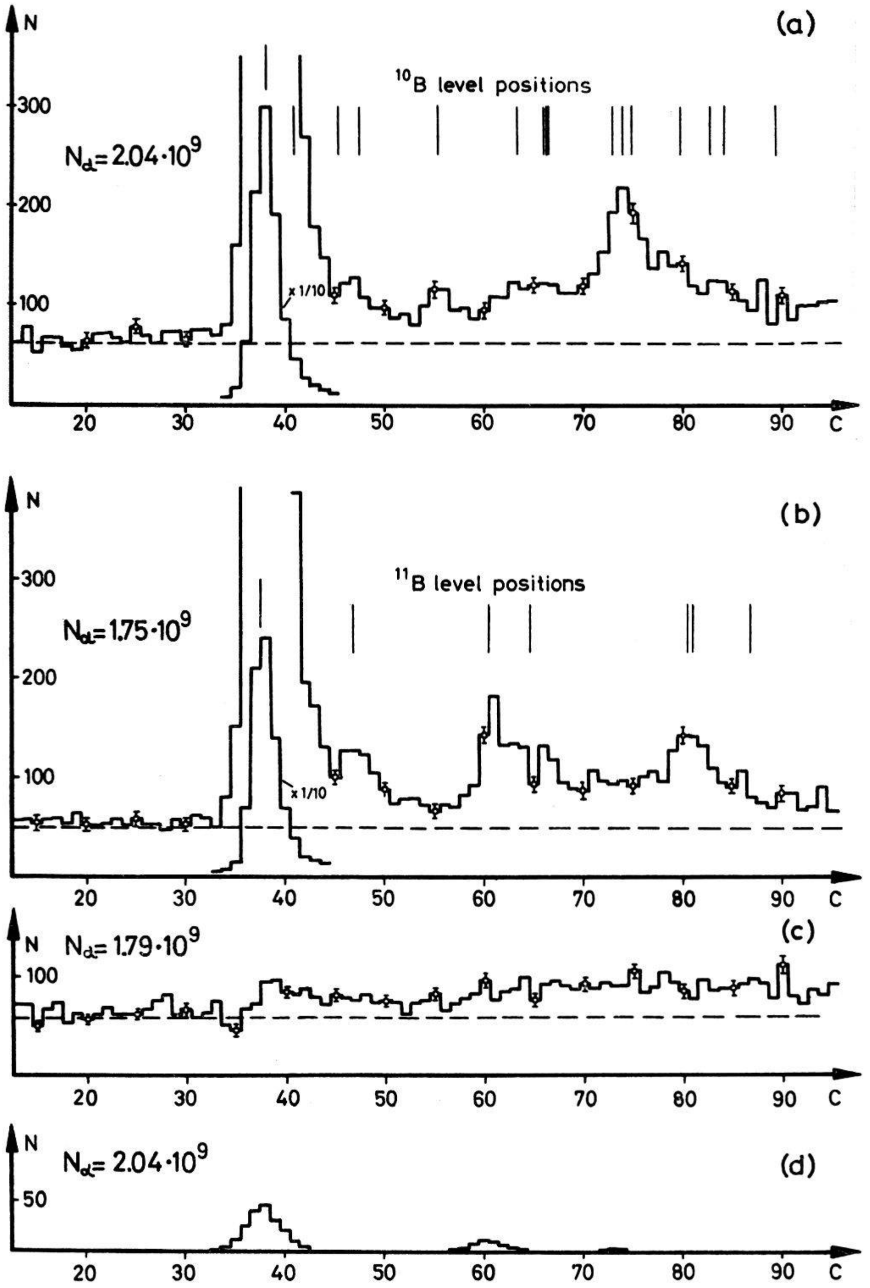

Figure 2
Time-of-flight spectra for $\phi_0 = 40°$ and a flight distance of 5 m:
a) Measured spectrum with ^{10}B-enriched scatterer.
b) Measured spectrum with natural boron scatterer.
c) Measured spectrum of the contribution from the environment (see text).
d) Calculated spectrum of the scattering by the enclosure and the impurities of the ^{10}B-enriched scatterer.
The dashed lines represent the accidental coincidence level.

As can be seen from Figure 2, the contribution from the environment to the total spectrum of a scatterer is significant. However, in measurements similar to ours, this contribution has hitherto always been neglected, thus leading to errors of a few mb/sr. Consequently, one can certainly suspect that this is the reason for the disagreement between the various measurements of neutron scattering to the $Q = -7.66$ MeV (2^+) level of ^{12}C [11–14]. One way of eliminating practically all of the contribution from the environment consists of shielding and collimating the neutron detector (closed geometry) [15]. However, such a shield introduces new parasitic events due to two successive interactions, the first in the scatterer, the second at the surface of the collimation channel. Estimation of the importance of these events is difficult. We have not found a technique for measuring their contribution and therefore decided to retain an open geometry and subtract the measured contribution from the environment.

4. Efficiency of the Neutron Detector

The efficiency at 14.15 MeV was determined by placing the detector in the neutron beam. For lower energies, it was measured by the technique of the scintillating hydrogen scatterer [13]. The number of neutrons of a given energy reaching the detector after simple or multiple scattering has been calculated by a Monte-Carlo program. Detection of the interaction in the scatterer (NE 102 A plastic scintillator) and selection of only those events producing the same amount of light as the simple scattering from hydrogen, made the contribution from the environment negligible ($< 0.5\%$).

Nevertheless, the above measuring technique presents two difficulties due to the poor amplitude resolution of the scintillating scatterer detector:

1. Special care in light collection must be taken to detect all good events in the scatterer, more particularly for small scattering angles when the recoil proton energy is low (amplitude resolution $> 100\%$).
2. When calculating the contribution from the multiple scattering events (4 to 6%, depending on ϕ_0) with the Monte-Carlo program, it is difficult to introduce the spectrometric selection on the scatterer.

In order to ascertain whether these two problems had been correctly solved, measurements were carried out without introducing the detection of the interaction in the scatterer, especially for $\phi_0 \leqslant 30°$. It was then necessary to take into account the contribution from the environment, which was no longer negligible, and to subtract the contribution from the ^{12}C in the scatterer, as estimated from auxiliary measurements. The statistical precision was thus not very good. The results, however, were in good agreement with those obtained with detection of the interaction in the scatterer. The average precision for the neutron detector efficiency is $\pm 2.5\%$.

5. Evaluation of Cross-Sections

5.1. *Elimination of the Contribution Due to the Minority Isotope in the Time-of-Flight Spectrum of a Scatterer*

For a given ϕ_0, the probability ${}^{S}P^{J}(Q_i, \phi_0)$ that a neutron hitting the scatterer J is scattered (simple scattering), per unit solid angle, in the direction of the center of the neutron detector, leaving the residual nucleus of isotope i in the state with energy of excitation Q, may be written:

$$^{S}P^{J}(Q_i, \phi_0) = \int_V d(\vec{d})\ e^{-\Sigma^J(E_0) r_0}\ \sigma(E_0, Q_i, \phi)\ \mathfrak{n}_i^J\ e^{-\Sigma^J(E_1) r_1}\ dV\ , \tag{1}$$

where

$d(\vec{d})$	is the probability per unit of surface for a neutron to arrive with the direction $\vec{d}$ at the entrance surface of the scatterer;
E_0, E_1	is the neutron energy before and after scattering;
r_0, r_1	is the neutron path inside the scatterer before and after scattering;
$\mathfrak{n}_i^J$	is the number of atoms per cm^3 of isotope i in scatterer J;
$\Sigma^{J(E)}$	is the total macroscopic cross-section of scatterer J at energy E;
$\sigma(E, Q_i, \phi)$	is the differential cross-section corresponding to level Q of isotope i, at energy E and for scattering angle ϕ; and
V	is the volume of the scatterer.

We can also write:

$$^{S}P^{J}(Q_i, \phi_0) = \sigma(E_0, Q_i, \phi_0)\ \mathfrak{n}_i^J\ a^J(Q_i, \phi_0)\ , \tag{2}$$

thus defining the factor $a^J(Q_i, \phi_0)$ which depends on the total macroscopic cross-section of scatterer J and on the energy of the neutrons before and after scattering.

In the time-of-flight spectra for boron scattering in the scatterer J, the number $^{S}N^{J}(Q_i, \phi_0)$ of simple scattering events to the level Q of isotope i is given by

$$^{S}N^{J}(Q_i, \phi_0) = {}^{S}P^{J}(Q_i, \phi_0)\ N_\alpha^J(\phi_0)\ \varepsilon(\overline{E}_1)\ G(\phi_0)\ , \tag{3}$$

where

$N_\alpha^J(\phi_0)$	is the number of α-particles detected during the measurement;
$G(\phi_0)$	contains the geometrical factors (proportion of the beam neutrons hitting the scatterer, neutron detector solid angle, etc.); and
$\varepsilon(\overline{E}_1)$	is the efficiency of the neutron detector at the average energy $\overline{E}_1$ of the neutron after scattering to the level Q.

If it were possible to extract the different values of $^{S}N^{J}(Q_i, \phi_0)$ directly from the measured spectra, the cross-sections $\sigma(E_0, Q_i, \phi_0)$ sought could be calculated from relations (2) and (3) above. This is not possible, for the following reasons:

a) the simple scattering events to each level of the two isotopes are superimposed, and

b) the multiple scattering is mixed with the simple scattering and its contribution is unknown.

To estimate the cross-sections, we first constructed two new spectra, for each ϕ_0, from the two measured spectra for boron scattering from each scatterer. These new spectra, which we shall call isotope spectra, contained only simple scattering events from one isotope, plus some multiple scattering events.

Let $n^J(\phi_0, c)$ be the number of counts in channel c of a time-of-flight spectrum measured with scatterer J. Since $G(\phi_0)$ does not depend upon the scatterer and $\varepsilon(\overline{E}_1)$

is identical for a given level in the spectra of both scatterers for the same ϕ_0, the isotope spectra can be constructed by carrying out, for each channel, the subtraction:

$$n_i(\phi_0, c) = n^J(\phi_0, c) - \frac{\boldsymbol{n}_{i'}^{J}\, a^J(Q_{i'}, \phi_0)\, N_\alpha^J(\phi_0)}{\boldsymbol{n}_{i'}^{J'}\, a^{J'}(Q_{i'}, \phi_0)\, N_\alpha^{J'}(\phi_0)}\, n^{J'}(\phi_0, c)$$

$$n_{i'}(\phi_0, c) = n^{J'}(\phi_0, c) - \frac{\boldsymbol{n}_{i}^{J'}\, a^{J'}(Q_{i}, \phi_0)\, N_\alpha^{J'}(\phi_0)}{\boldsymbol{n}_{i}^{J}\, a^{J}(Q_{i}, \phi_0)\, N_\alpha^{J}(\phi_0)}\, n^{J}(\phi_0, c)\,, \tag{4}$$

where the index ′ is used to distinguish between the scatterers or the isotopes, and the factors $a^J(Q_i, \phi_0)$ are to be determined for a continuous variation of Q in the energy domain analysed.

In a general way, the ratio $a^J(Q_i, \phi_0)/a^{J'}(Q_i, \phi_0)$ varies according to the region of the time-of-flight spectrum considered. In our particular case, we profited from the fact that the variation with energy of the total macroscopic cross-sections of the two scatterers is very similar. By appropriately compressing the powder of the scatterers, we could approximately satisfy

$$a^J(Q_i, \phi_0) = a^{J'}(Q_i, \phi_0) = a(Q_i, \phi_0)\,. \tag{5}$$

By introducing (5) in relation (4), the number ${}^SN(Q_i, \phi_0)$ of simple scattering events to the level Q in the spectrum of isotope i is found to be related to the cross-section by

$${}^SN(Q_i, \phi_0) = \sigma(E_0, Q_i, \phi_0)\, a(Q_i, \phi_0) \left(\boldsymbol{n}_i^J - \boldsymbol{n}_i^{J'} \frac{\boldsymbol{n}_{i'}^{J}}{\boldsymbol{n}_{i'}^{J'}}\right) N_\alpha^J(\phi_0)\, \varepsilon(\overline{E}_1)\, G(\phi_0)\,. \tag{6}$$

We have subsequently ascertained, with the use of a Monte-Carlo program to be described below, that the relation (5) was indeed satisfied. The few per cent difference obtained gives rise to no error as it only affects the fraction of the spectrum subtracted.

It is interesting to note that, in measurements similar to ours, carried out with two scatterers of different isotopic concentrations, relation (5) has hitherto been assumed valid, even when the macroscopic cross-sections of the scatterers were fairly different. The error thus committed can be significant when the volume of the scatterers is large [16, 17].

5.2. *Estimation of the Contribution from the Simple Scattering to Each Level in the Isotope Spectra*

The multiple scattering events in the isotope spectra represented an average of about 20% of the simple scattering events. To obtain a first approximation of the different ${}^SN(Q_i, \phi_0)$, we first extracted the contribution $N(Q_i, \phi_0)$ from both simple and multiple scattering events in the time range corresponding to the level considered. When the level was sufficiently isolated from its neighbours, we needed only sum up the contents of the associated channels. In the other cases, we assumed that the contribution from the level was contained within one peak, whose shape was supposed the same for each level. It is clear that this hypothesis deviates somewhat from reality. The shape of the peak corresponding to the simple scattering events depends upon the level itself, and the structure of the multiple scattering spectrum is more complicated. However, the error resulting from this choice was corrected for with a Monte-Carlo calculation. A standard peak shape was derived from auxiliary measurements of neutron scattering to the $Q = -4.43$ MeV (2^+) level of ^{12}C, and the $N(Q_i, \phi_0)$ were then computed, whenever possible, from a least-squares fit.

Once the different $N(Q_i, \phi_0)$ are known, the simple scattering events can be evaluated, to a first approximation, from the relation

$$^{S}N(Q_i, \phi_0) = \frac{N(Q_i, \phi_0)}{m(Q_i, \phi_0)}, \tag{7}$$

where the $m(Q_i, \phi_0)$ represent the contribution due to the multiple scattering events. Both the $m(Q_i, \phi_0)$ and the $a(Q_i, \phi_0)$, which at this stage in the data analysis cannot yet be given with precision, have been roughly estimated and a first approximation $\sigma^0(E_0, Q_i, \phi_0)$ of the cross-sections has been calculated using expression (6).

5.3. *Monte-Carlo Calculations*

The cross-sections $\sigma^0(E_0, Q_i, \phi_0)$ have been introduced into the Monte-Carlo program of Joseph et al. [13], which was developed for two isotopes and twenty levels and includes both the time resolution of the experimental apparatus and the efficiency of the neutron detector. This program reproduces the time-of-flight spectra of the scatterers which would have been measured if the cross-sections had really been $\sigma^0(E_0, Q_i, \phi_0)$. Besides the $\sigma^0(E_0, Q_i, \phi_0)$, the total macroscopic cross-sections of the scatterers and the differential cross-sections below 14 MeV must be introduced in the program. These were extracted from available theoretical or experimental data. When no data existed, especially for the inelastic differential cross-sections, they were deduced from our measurements at 14 MeV. The imprecision which is thus introduced is of no consequence, since these cross-sections only appear in the calculation of the multiple scattering events. The statistical accuracy of the Monte-Carlo calculation varies between 1 and 6%, according to the level considered.

The calculated spectra for each of the two scatterers were combined in exactly the same way as the measured spectra (equation 4). Figure 3 shows a comparison between the spectra thus obtained and the measured ones (isotope spectra). One can see that even in this first approximation the agreement is good. The calculated contribution from the multiple scattering is likewise plotted.

On the basis of the Monte-Carlo calculation, more precise values have been obtained for the $a(Q_i, \phi_0)$ and $m(Q_i, \phi_0)$. The error introduced by the choice of peak shape has been corrected for by comparison, in the isotope spectra resulting from the Monte-Carlo calculation, of the estimate of the contents of a peak on the basis of this shape and its actual contents, thus defining the corrective factor $f^*(Q_i, \phi_0)$. The first values $\sigma^0(E_0, Q_i, \phi_0)$ of the cross-sections were then corrected, using the relation

$$\sigma(E_0, Q_i, \phi_0) = \sigma^0(E_0, Q_i, \phi_0) \frac{a(Q_i, \phi_0)\, m(Q_i, \phi_0)}{a^*(Q_i, \phi_0)\, m^*(Q_i, \phi_0)\, f^*(Q_i, \phi_0)}, \tag{8}$$

where $a(Q_i, \phi_0)$ and $m(Q_i, \phi_0)$ result from the first approximation and $a^*(Q_i, \phi_0)$ and $m^*(Q_i, \phi_0)$ are taken from the Monte-Carlo calculation.

The difference between the cross-sections before and after correction was less than 10% for the most highly excited levels and less than 20% for the others. Considering the statistical error of the measurement, a second Monte-Carlo calculation to further improve the precision of the cross-sections was not justified.

The correction made by equation (8) can be considered in another way which leads to the same result: the isotope spectra given by the Monte-Carlo calculation can be analysed in exactly the same way as the measured spectra, using the same peak shape. Let $N^*(Q_i, \phi_0)$ be the contents obtained for the peaks associated with each of the levels. The correction indicated under (8) then reduces to

$$\sigma(E_0, Q_i, \phi_0) = \sigma^0(E_0, Q_i, \phi_0) \frac{N(Q_i, \phi_0)}{N^*(Q_i, \phi_0)}, \tag{9}$$

where $N(Q_i, \phi_0)$ is the value obtained from the measured spectra.

The estimation of the $N(Q_i, \phi_0)$ in the measured spectra has been performed in several ways, by considering all channels containing the simple scattering to one level (or one group of levels), or only some of these channels, around the maximum of the peak. For levels sufficiently distant from their neighbours, the standard-shape analysis result has been compared to that obtained by summing the contents of the channels considered. The position of the maximum of a peak was defined to within one-half of a channel, the average peak width being 9 channels. Tests have been made in which this maximum was displaced by half a channel. For all the different modes of analysis, the cross-sections, as obtained after appropriate correction by the Monte-Carlo calculation, did not differ by more than a few per cent.

Thus the above analysis, using a standard peak shape and Monte-Carlo calculation, (i) permits a significant improvement in the time resolution of the time-of-

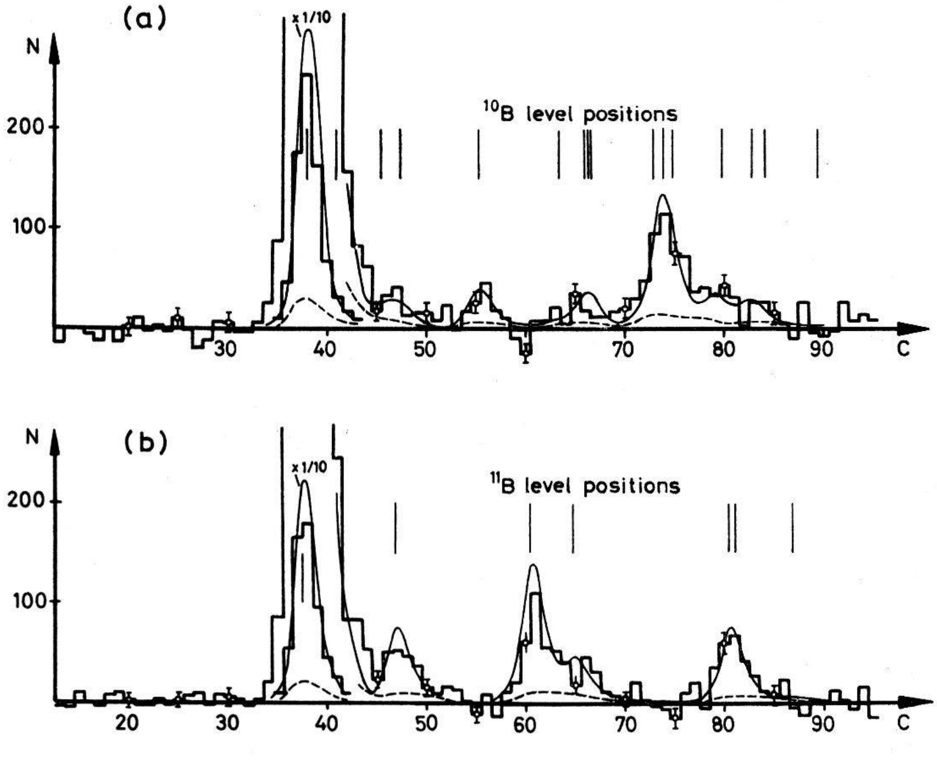

Figure 3
Isotope spectra for $\phi_0 = 40°$: a) ^{10}B; b) ^{11}B. The histograms are deduced from measurements. The continuous curves are the corresponding Monte-Carlo calculation results. Dashed curves represent the multiple scattering spectra only as calculated by the Monte-Carlo program.

flight spectrometer, (ii) allows an estimation of the contribution due to multiple scattering and (iii) furnishes a correction for finite geometry.

Another correction, not mentioned in the formulae of this paragraph, has been made for neutron interactions in the air between scatterer and detector.

The Monte-Carlo calculation has, moreover, permitted a verification of the technique employed to eliminate the contribution from the environment. In the spectra of the isotope ^{11}B (Fig. 3), some peaks are so well separated that only the multiple scattering appears in the interval between them plus the residual contribution from the environment, if any. An analysis has been carried out in such regions as if levels were located there: the cross-sections thus obtained were indeed zero, to within the statistical error.

6. Results

Only the results obtained for ^{10}B will be reported in this paper. Besides the elastic scattering, we have isolated the inelastic scattering to five levels. For three groups of levels, separation of the contributions to individual levels was not possible. The measured differential cross-sections are given in the center-of-mass system (scattering angle: θ_{CM}). They are reported in Figures 4, 5 and 6, or in Table I. The integrated cross-sections are listed in Table II. For the differential cross-sections, only statistical errors are reported. The other possible errors are considerably less important (approx. 5%). The error bounds are large for the $Q = -1.74$ MeV (0^+) and the $Q = -2.15$ MeV (1^+) levels because of their respective position in the time-of-flight spectra, namely in the tail of the elastic scattering peak. We have also listed in Table I the result of a determination of the cross-sections for these two levels together, whose precision is quite good. The precision given for the integrated cross-sections should be understood as including all the possible errors.

Table I

Measured differential cross-sections for some levels. Only the probable statistical errors ($\pm$ 0.675 $\times$ standard deviation) are given (other possible errors $\leqslant$ 5%)

	$Q =$ $-[1.74 + 2.15]$ MeV			$Q =$ -1.74 MeV (0^+)		$Q =$ -2.15 MeV (1^+)		$Q =$ -4.77 MeV (3^+)			$Q =$ $-[6.88\ (1^-)$ $+ 7.00]$ MeV		
ϕ_0 [°]	θ_{CM} [°]	σ [mb/sr]	$\Delta\sigma$	σ [mb/sr]	$\Delta\sigma$	σ [mb/sr]	$\Delta\sigma$	θ_{CM} [°]	σ [mb/sr]	$\Delta\sigma$	θ_{CM} [°]	σ [mb/sr]	$\Delta\sigma$
10	11.1	–	–	3.2	1.8	2.0	1.8	11.3	1.8	1.1	11.5	0.7	0.4
15	16.6	3.9	0.8	−0.8	1.5	2.2	1.5	16.9	1.8	0.8	17.2	0.8	0.3
27.5	30.3	3.7	0.6	0.7	1.2	1.4	1.2	31.0	0.7	0.6	31.4	0.1	0.4
40	44.0	1.8	0.3	1.2	0.7	2.5	0.7	44.8	0.2	0.3	45.4	0.8	0.2
52.5	57.5	1.5	0.3	1.5	0.7	0.2	0.7	58.4	0.3	0.3	59.2	1.1	0.3
65	70.7	0.9	0.2	0.2	0.7	0.1	0.7	71.7	0	0.3	72.6	0.7	0.3
77.5	83.6	0.8	0.2	1.3	0.7	0	0.7	84.7	0	0.3	85.7	1.3	0.3
90	96.3	0.9	0.2	−0.1	0.5	0.5	0.5	97.4	−0.5	0.6	98.4	–	–
102.5	108.6	1.0	0.2	0.6	0.5	0.4	0.5	109.7	0	0.2	110.7	1.1	0.3
115	120.7	0.4	0.2	0.2	0.5	0.1	0.5	121.7	0.5	0.3	122.6	−0.6	0.4
127.5	132.5	0	0.3	0.8	0.5	−1.2	0.5	133.4	0.8	0.4	134.2	2.4	0.8
140	144.0	0.5	0.3	0.8	0.5	−0.6	0.4	144.8	0.7	0.6	145.4	1.3	0.9
152.5	155.4	0.8	0.2	1.3	0.4	−0.1	0.4	156.0	0.5	0.3	156.4	1.3	0.4
161.8	163.8	−0.4	0.3	−0.2	0.4	0.8	0.4	164.1	0.7	0.3	164.5	0.8	0.7

Table II
Integrated cross-sections
^{a}) contains, but to a negligible extent, a fraction of the scattering to the $Q = -0.717$ MeV (1^+) level.
^{b}) result of a comprehensive analysis for the two levels together.

Q [MeV], J^π	$\sigma \pm \Delta\sigma$ [mb]	Q [MeV], J^π	$\sigma \pm \Delta\sigma$ [mb]
0 $(3^+)^{a)}$	972 ± 35	– 4.77 (3^+)	4.2 ± 1.6
– 1.74 (0^+)	8 ± 3	– [5.11 (2^-) + 5.16 (2^+) + 5.18 (1^+)]	13.5 ± 2
– 2.15 (1^+)	5 ± 3	– [5.92 (2^+) + 6.04 (4^+) + 6.13 (3^-)]	68 ± 4
– [1.74 + 2.15]$^{b)}$	14.5 ± 1.5	– 6.56	9 ± 1.5
– 3.58 (2^+)	11 ± 1.5	– [6.88 (1^-) + 7.00]	11 ± 1.5

To our knowledge, only one other measurement of the angular distribution of the differential cross-sections of neutrons scattered by ^{10}B has been published [3], but for neutrons of lower energy (7.5 MeV). On the other hand, many measurements exist of charged-particle scattering [18–22]. The group of levels $Q = -5.92\ (2^+)$, $-6.04\ (4^+)$ and -6.13 MeV (3^-) always appears to be the most highly excited. Considering the error bars, our results are in good agreement with those with which they are the most comparable, namely the data from proton scattering at incident energies between 10 and 17 MeV [18, 20]. Only for the $Q = -1.74$ MeV (0^+) level does the comparison fail: our cross-sections for this level are larger, but, on the other hand, our precision in this case is fairly poor.

7. Analysis of the Elastic Scattering with the Optical Model

Analysis of our data was performed using the program of Perey [23], for an optical potential of the form

$$V(r) = -V_C\, f(r, r_C, a_C) + 4\, i\, a_D\, V_D \frac{d}{dr} f(r, r_D, a_D) + \boldsymbol{\sigma} \cdot \boldsymbol{l} \left(\frac{\hbar}{m_\pi c}\right)^2 \frac{V_{so}}{r} \frac{d}{dr} f(r, r_{so}, a_{so}) \tag{10}$$

with

$$f(r, r_i, a_i) = \left(1 + \exp\left(\frac{r - r_i A^{1/3}}{a_i}\right)\right)^{-1}.$$

Several sets of values for the 9 potential parameters have been studied. The resulting curves are plotted in Figure 4 and compared with experimental results; the corresponding values of the parameters are listed in Table III. The best fit was first obtained without restricting the values assumed by the parameters, by minimizing the quantity

$$\chi^2 = \frac{1}{N} \sum_{i=1}^{N} \left(\frac{\sigma_{th}(\theta_i) - \sigma_{exp}(\theta_i)}{\Delta\sigma_{exp}(\theta_i)}\right)^2, \tag{11}$$

where $\sigma_{th}(\theta_i)$ and $\sigma_{exp}(\theta_i)$ are the theoretical and measured differential cross-sections, respectively, for the scattering angle θ_i, and $\Delta\sigma_{exp}(\theta_i)$ is the experimental error. N is the number of angles for which measurements have been carried out. The agreement between the experimental points and the calculated curve is good (Fig. 4, curve c),

Table III
Sets of parameters for optical potential and corresponding integrated cross-sections:
A) Standard parameters [15]
B) Best fit with standard values for r_i, a_i and V_{so}
C) Best fit without limitations on the 9 parameters

		A	B	C			A	B	C	Measured
V_C	[MeV]	44.0	48.12	56.75	r_{so}	[F]	1.25	1.25	1.26	
r_C	[F]	1.25	1.25	1.09	a_{so}	[F]	0.65	0.65	0.64	
a_C	[F]	0.65	0.65	0.63	σ_{el}	[b]		0.944	0.956	0.972 ± 0.035
V_D	[MeV]	9.6	6.43	10.75	σ_r	[b]		0.560	0.478	
r_D	[F]	1.25	1.25	1.59	σ_{tot}	[b]		1.504	1.434	1.45 ± 0.05
a_D	[F]	0.47	0.47	0.19	χ^2		190.0	40.0	4.97	
V_{so}	[MeV]	6.0	6.0	5.44						

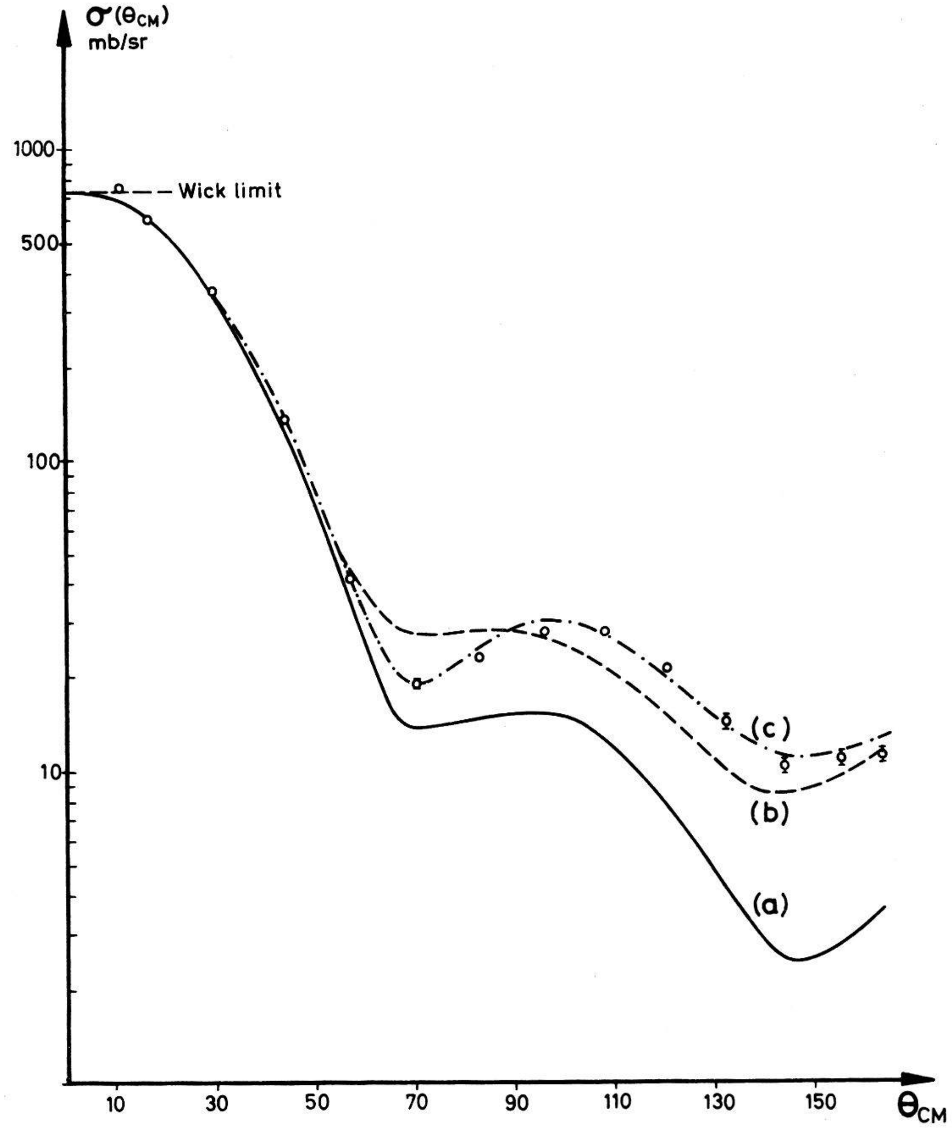

Figure 4
Elastic scattering. Comparison of the experimental results with the predictions of the optical model: curve a), optical model with standard parameter set (Table III, A),
curve b), optical model, best fit with standard values for r_i, a_i and V_{so} (Table III, B),
curve c), optical model, best fit without limitations on the 9 parameters of the potential (Table III, C).

but the values obtained for the parameters differ considerably from those (standard values) which are usually used with heavier nuclei [15]. It is nonetheless known [23] that, for structural reasons, the standard parameter values do not give good results for the light nuclei. The curve calculated with the standard values is also plotted in Figure 4 (curve a). It deviates noticeably from the experimental data for $\theta_{CM} > 60°$. A better fit, certainly the most 'realistic' one, has been obtained by keeping r_i, a_i and V_{so} fixed at the standard values and leaving V_C and V_D free (Fig. 4, curve b).

The values of the total and reaction cross-sections predicted by the optical model agree well with the experimental data (Table III). We have also plotted in Figure 4 the Wick limit [24], which is a lower bound for the cross-section at 0°. It is compatible with the measured values.

8. Analysis of the Inelastic Scattering with the DWBA-Collective Model

By assuming the collective nature of the excited states of ^{10}B, Squier et al. [22] were able to reproduce, within the framework of a distorted-wave Born approximation (DWBA), the results of their ^{3}He scattering measurements for a few levels. We have also analysed our own data with the DWBA program DWUCK developed by Kunz [25]. In the model considered, the correlated movements of the nucleons produce a static, axially symmetric deformation of the nucleus, whose surface is described by

$$R(\theta) = R_0 \left(1 + \sum_L \beta_L Y_L^0(\theta)\right). \tag{12}$$

The interaction potential depends only on the distance from the surface of the nucleus. It can be expanded in a Taylor series about $r = R_0$ to give

$$V\,(r - R(\theta)) = V\,(r - R_0) - \frac{d}{dr} V\,(r - R_0)\,\delta r + \frac{1}{2}\,\frac{d^2}{dr^2} V\,(r - R_0)\,\delta R^2 + \dots, \tag{13}$$

with

$$\delta R = R_0 \left(\sum_L \beta_L Y_L^0\,(\theta)\right).$$

The first term in this expansion is the non-deformed optical potential (equation 10) and gives rise to the elastic scattering. The inelastic scattering depends upon higher terms of which the second term is considered to be the most important, the others being neglected.

The data used by the DWUCK program are: (i) parameters of the optical potential, and (ii) the transferred angular momentum, L. The program takes into account the contribution to the scattering due to deformation of the imaginary part of the optical potential, but it does not include spin-orbit coupling.

For all levels which could be described by this model, the calculations were performed with the three sets of optical-potential parameters as defined in the analysis of the elastic scattering (Table III), and for each possible value, L, of the transferred angular momentum. We give below the results, beginning with the $Q = -3.58$ MeV level for which the experimental results are the most precise.

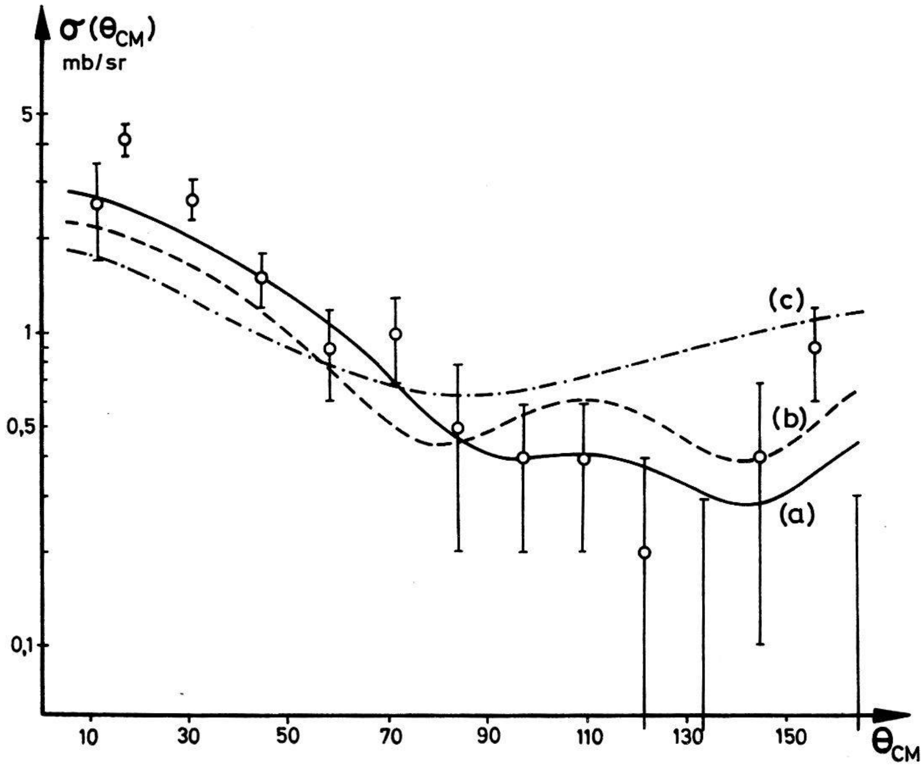

Figure 5
$Q = -3.58$ MeV (2^+) level. Comparison of the experimental results and the predictions of the DWBA-collective model for $L = 2$. Curves a, b and c correspond to sets A, B and C of optical potential parameters in Table III and to the deformation parameters $\beta_2 = 0.69$, 0.49 and 0.49, respectively.

$Q = -3.58$ MeV (2^+) level: The best fits have been obtained for $L = 2$. They are shown in Figure 5. The curve calculated with the standard optical potential parameters and $\beta_2 = 0.69$ gives the best agreement with the experimental values. The curve calculated with the most realistic parameters deduced from our analysis of elastic scattering (Table III, B) still fits the experimental results quite well ($\beta_2 = 0.49$). On the other hand, the curve calculated with the third set of parameters (Table III, C), which nonetheless described best the measured elastic scattering data, deviates noticeably from the experimental values. Squier et al. [22] have obtained a good fit for this level for $L = 2$ and $\beta_2 = 0.36$.

$Q = -1.74$ MeV (0^+) level: The scattering to this level involves a spin-flip process which cannot be described by the model.

$Q = -2.15$ MeV (1^+) level: Although experimental accuracy is poor, it can be noted that the curves calculated for $L = 2$ with the parameter sets A and B and the same deformation parameters as for the $Q = -3.58$ MeV level, are compatible with the experimental values.

$Q = -4.77$ MeV (3^+) level: None of the calculated curves agrees with the measured cross-sections. This level could have a structure too complicated [26] to be described by the model.

$Q = -5.11$ (2^-), -5.16 (2^+) and -5.18 (1^+) MeV levels: The $Q = -5.18$ MeV level must result from the excitation of two nucleons [18, 26] and thus contributes little to the measured cross-sections. We have reported in Figure 6 the curves calculated for

the $Q = -5.16$ MeV level, with $L = 2$, the parameter sets A and B, and the same deformation parameters as for the $Q = -3.58$ MeV level. They agree quite well with the experimental results for θ_{CM} between 10 and 100°. The discrepancy between the

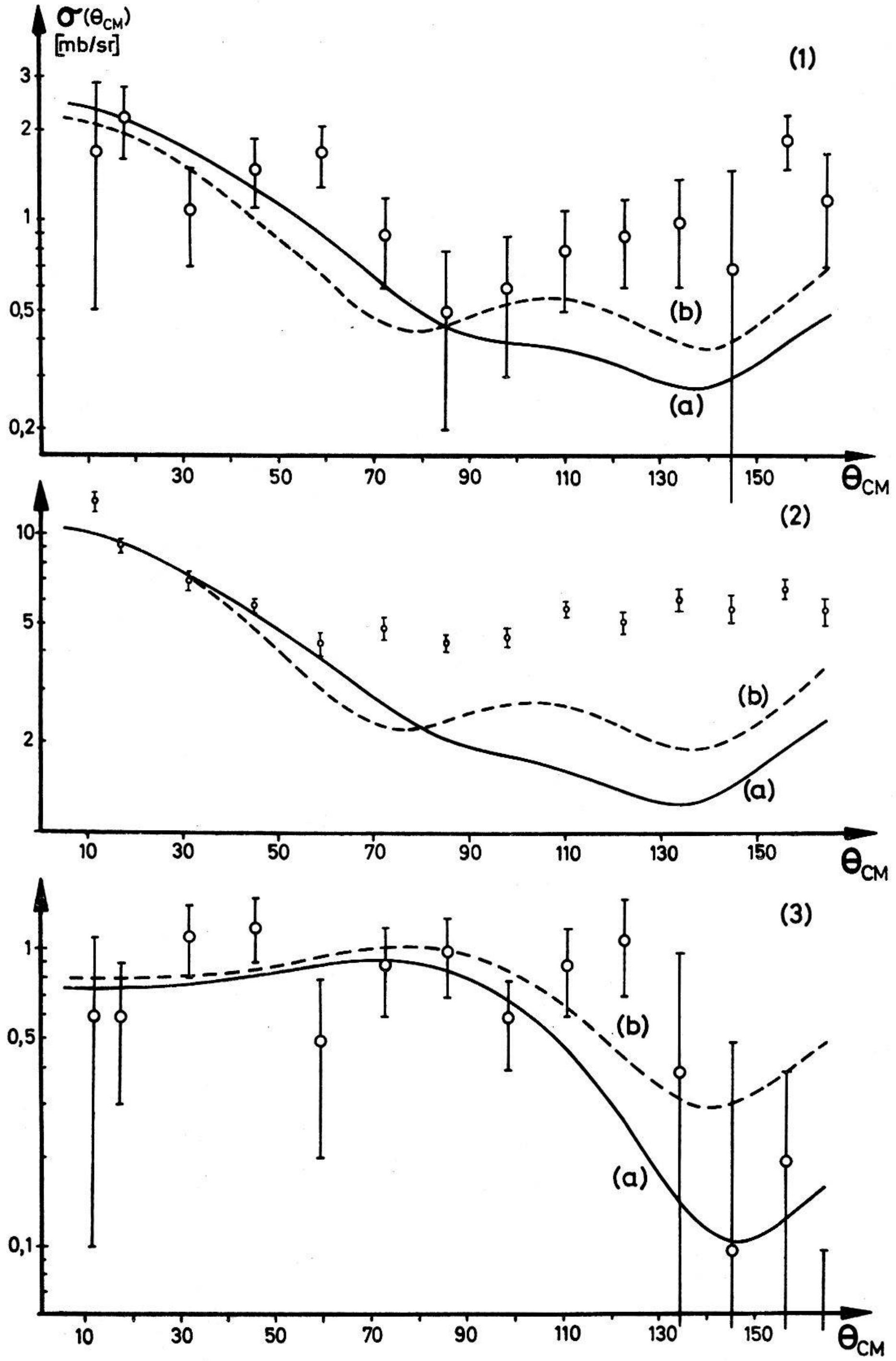

Figure 6

Comparison of the experimental results and the predictions of the DWBA-collective model. Curves a and b correspond to sets A and B of optical potential parameters in Table III.

1) $Q = -(5.11\ (2^-) + 5.16\ (2^+) + 5.18\ (1^+))$ MeV levels. Curves a and b have been calculated for the $Q = -5.16$ MeV level, with $L = 2$ and $\beta_2 = 0.69$ and 0.49, respectively.

2) $Q = -(5.92\ (2^+) + 6.04\ (4^+) + 6.13\ (3^-))$ MeV levels. Curves a and b have been calculated for the $Q = -6.04$ MeV level, with $L = 2$ and $\beta_2 = 1.1$ and 0.82, respectively.

3) $Q = -6.56$ MeV level. Curves a and b have been calculated for $L = 3$ (values of β_3 are given in the text).

theoretical curves and the measured values for $\theta_{CM} > 100°$ could be explained, to the extent that the model is applicable to the $Q = -5.16$ MeV level, by excitation of the $Q = -5.11$ MeV level.

$Q = -5.92$ (2^+), -6.04 (4^+) *and* -6.13 (3^-) *MeV levels:* By assuming that only the $Q = -6.04$ MeV level was excited, Squier et al. have obtained a good fit for $L = 2$, but with a deformation parameter $\beta_2 = 1.1$, i.e. considerably larger than for the other levels. The curves which we have calculated by making the same assumption do not agree with the experimental results (Fig. 6).

$Q = -6.56$ *MeV level:* The spin and parity of this level have not yet been established with certainty. The measured cross-sections agree well with the curves calculated for $L = 3$, which implies a negative parity (Fig. 6). The deformation parameter values obtained are, for parameter set A: $\beta_3 = 0.75$ if $J = 4$, $\beta_3 = 1.0$ if $J = 2$, and, for parameter set B: $\beta_3 = 0.62$ if $J = 4$, $\beta_3 = 0.83$ if $J = 2$.

In summary, the DWBA-collective model furnishes a coherent description of the inelastic scattering for the $Q = -2.15$, -3.58, -5.16 and -6.56 MeV levels. The best fits are obtained with the standard parameters of the optical potential (Table III, A) which, however, yield a much less satisfactory description of the elastic scattering. Only slightly different and still-valid fits are obtained with the most realistic parameters which can be extracted from our elastic scattering data (Table III, B). It is thus possible to find a set of parameters for the optical potential which describes simultaneously and satisfactorily both the elastic and inelastic scattering for a few excited levels. However, this set of parameters neither gives the best description of the elastic scattering nor of the inelastic scattering.

Conclusion

Special efforts in data analysis have extended the possibilities for neutron scattering measurements using a mixed-isotope target. The separation of overlapping peaks has been improved. Careful measurement of parasitic effects allow the determination of cross-sections smaller than one mb/sr.

The angular distributions of the differential cross-sections for elastic and inelastic neutron scattering at 14.1 MeV by ^{10}B have thus been measured for the first time. The results obtained have permitted the application of the optical model and of the DWBA-collective model to scattering by this nucleus. The collective nature of the $Q = -2.15$ MeV (1^+) and $Q = -3.58$ MeV (2^+) levels has been confirmed. It seems probable that the $Q = -5.16$ MeV (2^+) and $Q = -6.56$ MeV levels are also of a collective nature and that the parity of the $Q = -6.56$ MeV level, still poorly defined, is negative.

We would like to thank Professor Ch. Haenny for his advice and unfailing interest in this work. We are grateful to Drs A. Henchoz and J. F. Loude for their valuable collaboration. We also thank Drs M. Châbre and Y. Dupont for helpful discussions on the use of theoretical programs. Finally, we are undebted to the Swiss National Fund for Scientific Research for its financial support.

REFERENCES

[1] K. Tesch, Nucl. Phys. *37*, 412 (1962).
[2] A. J. Frasca, R. W. Finlay, R. D. Koshel, R. L. Cassola, Phys. Rev. *144*, 854 (1966).
[3] J. C. Hopkins, D. M. Drake, Nucl. Sci. Ing. *36*, 275 (1969).
[4] M. Rahman, A. Banerjee, H. M. Sen Gupta, Ann. Phys. *49*, 320 (1968).
[5] Compilation of EANDC Request, EANDC 43 'U', avr. 1965.
[6] J. C. Alder, B. Vaucher, to be published. in Nucl. Phys.
[7] B. Vaucher, thèse, Ecole Polytechnique Fédérale de Lausanne, 1969.
[8] J. C. Alder, thèse, Ecole Polytechnique Fédérale de Lausanne, 1969.
[9] A. Henchoz, C. Joseph, Helv. phys. Acta *38*, 663 (1965).
[10] G. A. Grin, C. Joseph, Nucl. Instr. Meth. *24*, 331 (1963).
[11] R. Bouchez, J. Duclos, P. Perrin, Nucl. Phys. *43*, 628 (1963).
[12] R. L. Clarke, W. G. Cross, Nucl. Phys. *53*, 177 (1964).
[13] C. Joseph, G. A. Grin, J. C. Alder, B. Vaucher, Helv. phys. Acta *40*, 693 (1967).
[14] G. A. Grin, B. Vaucher, J. C. Alder, C. Joseph, Helv. phys. Acta, *42*, 990 (1969).
[15] P. H. Steltson, R. L. Robinson, H. J. Kim, J. Rapaport, G. R. Satchler, Nucl. Phys. *68*, 97 (1965).
[16] G. C. Bonnazola, E. Chiavassa, T. Bressani, Nucl. Phys. *86*, 378 (1966) and Nuovo Cim. *45*, 1B, 60 (1966).
[17] J. H. Towle, Nucl. Phys. A *100*, 257 (1967).
[18] G. Schrank, E. K. Warburton, W. W. Daehnick, Phys. Rev. *127*, 2159 (1962).
[19] B. H. Armitage, R. E. Meads, Nucl. Phys. *33*, 494 (1962) and Phys. Lett. *8*, 346 (1964).
[20] R. E. Segel, P. P. Singh, S. A. Hanna, M. A. Grace, Phys. Rev. *145*, 736 (1966).
[21] W. Fitz, R. Jahr, R. Santo, Nucl. Phys. A *101*, 449 (1967).
[22] G. T. A. Squier, E. A. Mc Clatchie, A. R. Johnston, R. J. Batten, J. B. A. England, F. G. Kingston, Nucl. Phys. A *119*, 369 (1968).
[23] F. G. Perey, Phys. Rev. *131*, 745 (1963).
[24] G. C. Wick, Atti. Acad. d'Ital. *13*, 1203 (1943).
[25] P. D. Kunz, University of Colorado, unpublished.
[26] D. E. Alburger, P. D. Parker, O. J. Bredin, D. H. Wilkinson, P. F. Donovan, A. Gallmann, R. E. Pixley, L. F. Chase jr., R. E. Mc Donald, Phys. Rev. *143*, 692 (1966).